Optica Applicata, Vol. XLIV, No. 4, 2014
DOI: 10.5277/oa140412

Modeling and optimization of the YAG:Yb microchip laser passively *Q*-switched by YAG:Cr absorber

OLEH BURYY*, SERHIJ UBIZSKII

Department of Semiconductor Electronics, Lviv Polytechnic National University, Bandery 12, 79646 Lviv, Ukraine

*Corresponding author: crystal@polynet.lviv.ua

Based on analytical and numerical solutions of the rate equations system and the heat conductivity equation, the model of the quasi-three-level passively *Q*-switched YAG:Yb/YAG:Cr microchip laser is developed. The obtained results are used for its optimization, *i.e.*, for the determination of the output mirror reflectivity, the pumping beam radius, the thickness of the absorber and the phototropic centers concentration maximizing the energy in the laser pulse. The influence of the thermal load on the spatial parameters of the laser beam is also determined.

Keywords: Yb:YAG crystal, microlaser, *Q*-switching, numerical simulation.

1. Introduction

Recently the passively *Q*-switched microchip lasers are widely investigated and developed as compact sources of the relatively high-power radiation for the systems of communications, ranging, medicine, robotics, *etc*. Such a laser consists of the generating medium, the saturable absorber and the mirrors formed on the laser crystal edges. The submillimeter length of these lasers allows to ensure the single-frequency and single-mode generation. The yttrium-aluminium garnet $Y_3Al_5O_{12}$ (YAG) crystal doped by Nd is often used as the active medium of microchip lasers. At the same time, the YAG crystal doped by Yb is characterized by the number of advantages that make it attractive for using in the *Q*-switched lasers in comparison with YAG:Nd. Particularly, it is characterized by a wider absorption band in the pumping region [1], lower Stokes' losses, higher lifetime of the upper laser level [2], the insignificance of the concentration quenching [3], the wide emission band that allows frequency tuning and short pulses generation [4], the absence of the upconversion and excited state absorption (ESA) processes [5]. The effective laser transition cross-section of YAG:Yb is relatively low: it is equal to 2.1×10^{-20} cm^2 for the wavelength of 1030 nm and to 0.31×10^{-20} cm^2 for 1050 nm [3]. However, it may be the advantage in the case of *Q*-switched lasers be-

cause the relatively low amplification allows to increase the energy in the laser pulse due to an increase in the inversion before irradiation.

Pumping of YAG:Yb is carried out on the wavelengths of 940–941 nm [6, 7] or 968–970 nm [1, 8]. Here we assume that the laser is edge pumped by laser diodes on 940 nm and generates on 1030 nm that corresponds to the laser investigated in [6].

The main difference between the microchip lasers based on YAG:Nd and YAG:Yb is the quasi-three-level generation scheme of YAG:Yb (Fig. 1**a**).

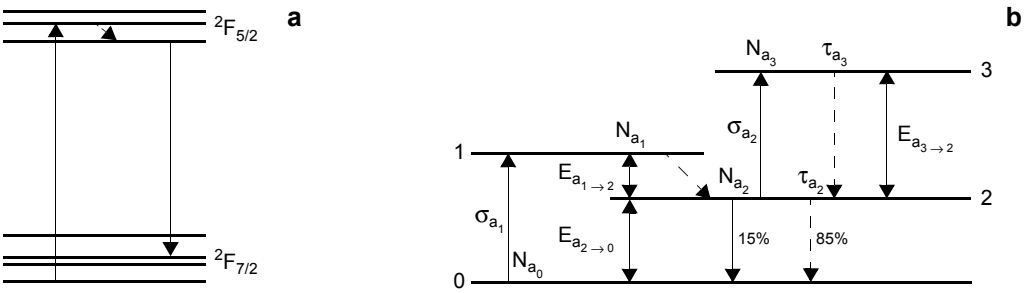

Fig. 1. Energy levels of Yb^{3+} ions (**a**) and phototropic centers – $Cr^{4+}(d)$ ions (**b**) in YAG. The solid and the dashed lines correspond to the radiative and non-radiative transitions, respectively.

The upper sublevels of the ground manifold $^2F_{7/2}$ is placed on the distances of 565, 612 and 785 cm^{-1} from the lowest Stark' sublevel and the upper sublevels of the manifold $^2F_{5/2}$ – on 297 and 352 cm^{-1} from its lowest sublevel. At the room temperature the occupations of the sublevels of the $^2F_{7/2}$ manifold are about 87.5%, 5.8%, 4.7% and 2.0% from the total quantity of Yb^{3+} ions. An increase in temperature on 100 K leads to a decrease in the lowest sublevel occupation on ~10%. So the influence of heating on the parameters of YAG:Yb is not too significant, what allows to describe the laser action in the frames of the fourth-level models as it is realized in [6, 9, 10]. However, such an approach is obviously doubtful in all possible cases. So the aim of our work is developing of the YAG:Yb/YAG:Cr microchip laser model taking into account the quasi-three-level character of the generation scheme as well as the elaboration of the optimization procedure of YAG:Yb/YAG:Cr microchip laser analogous to the one proposed earlier for the fourth-level microchip lasers [10].

2. Modeling of the YAG:Yb/YAG:Cr microchip laser

The model of YAG:Nd/YAG:Cr laser based on solutions of the rate equations is well known [11, 12]. However in the case of YAG:Yb/YAG:Cr it should be generalized by taking into account the thermal occupations of the levels as well as the non-radiative transitions between the levels of an absorber that, in turn, allows to determine the thermal load and its influence on the parameters of radiation. Designating the concentrations of Yb^{3+} ions on $^2F_{7/2}$ and $^2F_{5/2}$ manifolds as N_{g_l} and N_{g_u}, the concentrations of

$Cr^{4+}(d)$ ions on the corresponding levels (see Fig. 1**b**) as N_{a_0}, N_{a_1}, N_{a_2}, N_{a_3} and the quantity of photons in as q, one can obtain the expressions for their temporal changes:

$$\frac{\mathrm{d}N_{g_u}}{\mathrm{d}t} = R - \frac{N_{g_u}}{\tau_g} - \frac{\sigma_g c_0}{V'} q(f_{u_1} N_{g_u} - f_{l_3} N_{g_l}) \tag{1a}$$

$$N_{g_l} + N_{g_u} = N_{g_{\text{total}}} \tag{1b}$$

$$\frac{\mathrm{d}N_{a_0}}{\mathrm{d}t} = \frac{N_{a_2}}{\tau_{a_2}} - \frac{\sigma_{a_1} c_0}{V'} q(N_{a_0} - N_{a_1}) \tag{1c}$$

$$\frac{\mathrm{d}N_{a_1}}{\mathrm{d}t} = -\frac{N_{a_1}}{\tau_{a_1}} + \frac{\sigma_{a_1} c_0}{V'} q(N_{a_0} - N_{a_1}) \tag{1d}$$

$$\frac{\mathrm{d}N_{a_3}}{\mathrm{d}t} = -\frac{N_{a_3}}{\tau_{a_3}} + \frac{\sigma_{a_2} c_0}{V'} q(N_{a_2} - N_{a_3}) \tag{1e}$$

$$N_{a_0} + N_{a_1} + N_{a_2} + N_{a_3} = N_{a_{\text{total}}} \tag{1f}$$

$$\frac{\mathrm{d}q}{\mathrm{d}t} = \Big[2\sigma_g l_g (f_{u_l} N_{g_u} - f_{l_3} N_{g_l}) - 2\sigma_{a_1} l_a (N_{a_0} - N_{a_1}) + \\ - 2\sigma_{a_2} l_a (N_{a_2} - N_{a_3}) - 2\gamma\Big] \frac{q}{t_r} + \varepsilon (f_{u_l} N_{g_u} - f_{l_3} N_{g_l} + N_{g_{\text{total}}}) c_0 \sigma_g \frac{l_g}{l'} \tag{1g}$$

Here, Eqs. (1a) and (1b) describe the changes of the $^2F_{5/2}$ manifold occupation due to spontaneous and stimulated transitions as well as to pumping with the rate $R = P_a(A l_g h\nu_p)^{-1}$, where $A = \pi w_p^2$ is the pumping beam cross-section, w_p is the pumping beam radius, P_a is the pumping power absorbed in the active medium connected with the pumping power falling into the crystal P_i by expression $P_a = P_i[1 + \exp(-\alpha_g l_g + - 2\alpha_a l_a)][1 - \exp(-\alpha_g l_g)]$, α_g, α_a are the absorption coefficients in the generating medium (g) and the absorber (a), $P_a \approx P_i[1 - \exp(-2\alpha_g l_g)]$ if the absorber is isolated from the generating medium by reflecting coat, $\alpha_g = \sigma_p N_{g_{\text{total}}}$, σ_p is the absorption cross-section at the pumping wavelength, $\sigma_p = 8\times10^{-21}$ cm^2, $N_{g_{\text{total}}}$ is the concentration of the Yb^{3+} ions, l_g is the generating medium thickness, $h\nu_p$ is the energy of the pumping quantum, τ_g is the lifetime of the upper laser level, $\tau_g = 0.951$ ms, σ_g is the cross-section of the laser transition, $\sigma_g = 3.27\times10^{-20}$ cm^2. Equations (1c)–(1e) describe the processes in the absorber, *i.e.*, the absorption and the spontaneous transitions between the levels. The last equation describes the process of photons accumulation in the resonator. Here $V' = (l'/l_g)V_g$ is the effective mode volume, $l' = n(l_g + l_a)$ is the resonator optical length, l_a is the absorber thickness, usually $l_a \sim 10$–250 μm, V_g is the mode vol-

ume in the generating medium, $V_g = 0.25\pi w^2 l_g$, w is the radius of the laser beam waist, $N_{a_{\text{total}}}$ is the concentration of the phototropic centers, *i.e.*, the Cr^{4+} ions occupying the tetrahedral (d) positions in garnet lattice, N_{a_i}, τ_{a_i} are the concentration of the $Cr^{4+}(d)$ ions on the i-th level (see Fig. 1**b**) and its lifetime correspondingly, σ_{a_1} and σ_{a_2} are the cross-sections of transitions between the levels of $Cr^{4+}(d)$, $\sigma_{a_1} = 2.4\times10^{-18}$ cm^2, $\sigma_{a_2} = 2.8\times10^{-19}$ cm^2, $t_r = 2l'/c_0$ is the time of the double passing of the resonator, $\tau_c = l'/c_0\gamma$, $\gamma = \gamma_i + 0.5(\gamma_1 + \gamma_2)$ are the losses, γ_1, γ_2 are the losses on mirrors connected with their reflectivities R_1, R_2 by expressions $\gamma_1 = -\ln(R_1)$, $\gamma_2 = -\ln(R_2)$ (further $\gamma_1 = 0$), $\gamma_i = \alpha l$ is the loss in the active medium, α is the absorption coefficient at the laser wavelength, $\alpha \approx 0.005$ cm^{-1}, l is the resonator length, ε is the dimensionless coefficient characterising the comparative power of the spontaneous radiation, $\varepsilon = 10^{-13}$. The quantity of photons q is concerned with the output power by the expression $P(t) = h\nu t_r^{-1}\ln(R_2^{-1})q(t)$, ν is a radiation frequency. The energy in the laser pulse can be calculated as $E = \int P(t)\mathrm{d}t$, where the integral limits are determined by the pulse duration. The Boltzmann' factors

$$f_{l_3} = \frac{\exp\left[-(E_3 - E_1)/kT\right]}{\sum_{i=1}^{4}\exp\left[-(E_i - E_1)/kT\right]} \tag{2a}$$

$$f_{u_1} = \frac{1}{\sum_{i=1}^{3}\exp\left[-(E_i - E_1)/kT\right]} \tag{2b}$$

depend on the temperature and, consequently, on the heating power in the crystal. This power is determined by the intensity of the non-radiative transitions which are the higher, the higher are the upper levels occupations. In turn, the occupations depend on Boltzmann' factors as it follows from Eqs. (1a)–(1g). Thus, the correct solving of the system requires the iterative scheme analogous to the one used for thulium lasers [13] and consists of the following steps:

1) At the given value of the temperature, initially 25°C, the occupations of the levels and the power density Q are defined.

2) At the calculated value of the power density Q, the temperature distribution in the laser is determined from the non-stationary heat conductivity equation

$$\frac{\partial T}{\partial t} = a\left(\frac{\partial^2 T}{\partial x^2} + \frac{\partial^2 T}{\partial y^2} + \frac{\partial^2 T}{\partial z^2}\right) + \frac{Q(x, y, z, t)}{c_T\rho} \tag{3}$$

where c_T is the crystal specific heat, ρ is the density, a is the temperature conductivity, $a = \lambda_T c_T^{-1}\rho^{-1}$, λ_T is the heat conductivity. The form of the laser crystal is rectangular with dimensions $2a_x\times2a_y\times l$. The Boltzmann' factors are calculated at the temperature on the crystal axis obtained after averaging on the generating medium length T_{aver}.

3) If the difference between the temperature T_{aver} and its previous value (25°C for the first iteration) is more than 0.1°C, steps 1 and 2 are repeated; otherwise, the thermal calculation is finished and the laser parameters, *i.e.*, the peak power P_{max}, the energy E, the pulse duration $t_i = E/P_{max}$, the repetition rate F, are calculated from system (1).

In the step 1 the power density Q is determined from the following reasons. Because pumping is continuous, it leads to an increase in the concentration of Yb^{3+} ions on the upper manifold by the value of R during the unit of time. All excited ions distribute between the levels of the upper manifold in accordance with Boltzmann' distribution, at that $f_{u_1}R$ ions come to the upper laser level (the lowest sublevel of $^2F_{5/2}$ manifold). Each such a transition is accompanied by the liberation of the energy of $E_{u_{2\to 1}} =$ = 37 meV and, consequently, the heating power corresponding to this transition is equal to $V_g E_{u_{2\to 1}} f_{u_1} R$. Some part of the ions comes to the upper sublevel of the manifold; it leads to absorption of the power of $V_g E_{u_{3\to 2}} f_{u_3} R$, where f_{u_3} is the Boltzmann' factor of the upper sublevel, $E_{u_{3\to 2}}$ is the energy distance between the second and the third sublevels. Thus, the full heating power liberated due to these processes is $P_{g_u} = V_g R(E_{u_{2\to 1}} f_{u_1} - E_{u_{3\to 2}} f_{u_3})$. Simultaneously, pumping leads to a decrease in Yb^{3+} ions concentration on the lowest level of $^2F_{7/2}$ manifold that also causes the redistribution of the ions between the sublevels. This process is connected with liberation of the power $P_{g_l} = V_g R(E_{l_{2\to 1}} f_{l_2} + E_{l_{3\to 1}} f_{l_3} + E_{l_{4\to 1}} f_{l_4})$, where f_{l_2}, f_{l_3}, f_{l_4} are the Boltzmann' factors for the corresponding sublevels of the $^2F_{7/2}$ manifold, $E_{l_{i\to 1}}$ is the energy distance between i-th sublevel and the lowest one. Moreover, the concentration of the Yb^{3+} ions on $^2F_{7/2}$ manifold increases due to transition of the excited ions on the lower laser level that is the third Stark' sublevel of the $^2F_{7/2}$ manifold. Its occupation increases as

$$\frac{\mathrm{d}N_{l_3}}{\mathrm{d}t} = \frac{N_{g_u}}{\tau_g} + \frac{\sigma_g c_0}{V'} q(f_u N_{g_u} - f_l N_{g_l}) = R - \frac{\mathrm{d}N_{g_u}}{\mathrm{d}t} \tag{4}$$

and, in accordance with Boltzmann' distribution, the f_{l_4} part of these ions comes to the fourth level of the manifold, f_{l_2} – to the second and f_{l_1} – to the first one. The total heating power in the generating medium caused by all mentioned processes is

$$\begin{aligned} P_g(t) = V_g \Big\{ & R[E_{u_{2\to 1}} f_{u_1} - E_{u_{3\to 2}} f_{u_3} + E_{l_{2\to 1}} f_{l_2} + \\ & + E_{l_{3\to 1}}(f_{l_1} + f_{l_3}) + E_{3\to 2} f_{l_2} + E_{l_{4\to 1}} f_{l_4} - E_{3\to 4} f_{l_4}] + \\ & - (E_{l_{3\to 1}} f_{l_1} + E_{3\to 2} f_{l_2} - E_{3\to 4} f_{l_4}) \frac{\mathrm{d}N_{g_u}}{\mathrm{d}t} \Big\} \end{aligned} \tag{5}$$

Similarly, the heating power in the absorber is determined by the intensities of the transitions from upper levels of $Cr^{4+}(d)$ ions to lower ones

$$P_a(t) = V_a\left[E_{a_{1\to 2}}\frac{N_{a_1}(t)}{\tau_{a_1}} + E_{a_{3\to 2}}\frac{N_{a_3}(t)}{\tau_{s_3}} + E_{2\to 0}\frac{N_{a_2}(t)}{\tau'_{a_2}}\right] \tag{6}$$

where $V_a = 0.25\pi w^2 l_a$, τ'_{a_2} is the non-radiative lifetime of the level 2, $\tau'_{a_2} = 4.1$ μs.

Under the assumption that the pumping beam has got the Gaussian' profile with a beam waist of w_p, the power density $Q(r, z, t) \equiv Q(x, y, z, t)$ can be expressed from the heating powers in the generating medium and the absorber as follows:

$$Q(r, z, t) = \frac{2P_T(z, t)}{\pi\rho_0^2 l_m(z)}\exp\left(-\frac{2r^2}{w_p^2}\right) \tag{7}$$

where $P_T(z, t)$ is the power of heating sources, and

$$l_m(z) = \begin{cases} l_g, & 0 \le z \le l_g \\ l_a, & l_g < z \le l_g + l_a \end{cases} \tag{8}$$

For simplicity we assume that the temporal dependence of P_T can be presented as the sequence of the rectangular pulses

$$P_T(z, t) = \begin{cases} P_{g_{st}}, & 0 \le z \le l_g \\ 0, & l_g < z \le l_g + l_a \end{cases} \tag{9}$$

at the absence of generation, and

$$P_T(z, t) = \begin{cases} P_{g_{\max}}, & 0 \le z \le l_g \\ P_{a_{\max}}, & l_g < z \le l_g + l_a \end{cases} \tag{10}$$

at its presence. Here $P_{g_{\max}}$, $P_{a_{\max}}$ are the peak powers of the heat generation pulses.

At the known heating power density $Q(r, z, t)$, the stationary distribution of the temperature in the laser can be obtained from the heat conductivity equation by the integral transformations method. Designating the Biot' numbers as $Bi_x = \alpha_T\lambda_T^{-1}a_x$, $Bi_y = \alpha_T\lambda_T^{-1}a_y$, $Bi_z = \alpha_T\lambda_T^{-1}l$, where α_T is the heat transfer coefficient, $\alpha_T \approx$ ≈ 50 Wm^{-2}K^{-1} for convective cooling,

$$I_{x_i} = \int_{-a_x}^{a_x}\exp\left(-\frac{2x^2}{w_p^2}\right)\cos\left(\frac{\lambda_i x}{a_x}\right)\mathrm{d}x \tag{11a}$$

$$I_{y_j} = \int_{-a_y}^{a_y}\exp\left(-\frac{2y^2}{w_p^2}\right)\cos\left(\frac{\mu_j y}{a_y}\right)\mathrm{d}y \tag{11b}$$

where λ_i, μ_j, ν_k are the roots of equations obtained from the boundary conditions, $\tan(\lambda_i) = Bi_x\lambda_i^{-1}$, $\tan(\mu_j) = Bi_y\mu_j^{-1}$, $\tan(\nu_k) = 2\nu_k Bi_z(\nu_k^2 + Bi_z^2)^{-1}$, one can obtain:

$$T(r,z) = T_e + \frac{4}{\pi\lambda w_p^2 a_x a_y}\sum_{i,j,k=1}^{\infty} X_1\left[X_2(X_3+X_4)+X_5X_6\right]X_7 \tag{12}$$

where

$$X_1 = \frac{\lambda_i^2+Bi_x^2}{\lambda_i^2+Bi_x^2+Bi_x}\,\frac{\mu_j^2+Bi_y^2}{\mu_j^2+Bi_y^2+Bi_y}\,\frac{\nu_k^2}{\nu_k^2+Bi_z^2+2Bi_z}\,\frac{I_{x_i}I_{y_j}}{\frac{\lambda_i^2}{a_x^2}+\frac{\mu_j^2}{a_y^2}+\frac{\nu_k^2}{l^2}}$$

$$X_2 = \frac{1}{l_g}\left\{\sin\left(\frac{\nu_g l_g}{l}\right)-\frac{Bi_z}{\nu_k}\left[\cos\left(\frac{\nu_k l_g}{l}\right)-1\right]\right\}$$

$$X_3 = P_{g_{\max}}\left\{\exp\left[-a\left(\frac{\lambda_i^2}{a_x^2}+\frac{\mu_j^2}{a_y^2}+\frac{\nu_k^2}{l^2}\right)t_i\right]-1\right\}$$

$$X_4 = \bar{P}_g\left\{\exp\left[-a\left(\frac{\lambda_i^2}{a_x^2}+\frac{\mu_j^2}{a_y^2}+\frac{\nu_k^2}{l^2}\right)\frac{1}{F}\right]-\exp\left[-a\left(\frac{\lambda_i^2}{a_x^2}+\frac{\mu_j^2}{a_y^2}+\frac{\nu_k^2}{l^2}\right)t_i\right]\right\}$$

$$X_5 = \frac{1}{l_a}\left\{\sin(\nu_k)-\sin\left(\frac{\nu_k l_g}{l}\right)-\frac{Bi_z}{\nu_k}\left[\cos(\nu_k)-\cos\left(\frac{\nu_k l_g}{l}\right)\right]\right\}$$

$$X_6 = P_{a_{\max}}\left\{\exp\left[-a\left(\frac{\lambda_i^2}{a_x^2}+\frac{\mu_j^2}{a_y^2}+\frac{\nu_k^2}{l^2}\right)t_i\right]-1\right\}$$

$$X_7 = \frac{1-\exp\left[-a\left(\frac{\lambda_i^2}{a_x^2}+\frac{\mu_j^2}{a_y^2}+\frac{\nu_k^2}{l^2}\right)t\right]}{\exp\left[a\left(\frac{\lambda_i^2}{a_x^2}+\frac{\mu_j^2}{a_y^2}+\frac{\nu_k^2}{l^2}\right)\frac{1}{F}\right]-1}\cos\left(\frac{\lambda_i x}{a_x}\right)\cos\left(\frac{\mu_j y}{a_y}\right)\times$$

$$\times\left[\cos\left(\frac{\nu_k z}{l}\right)+\frac{Bi_z}{\nu_k}\sin\left(\frac{\nu_k z}{l}\right)\right]$$

The insignificant temperature changes between the laser pulses generation are neglected in Eq. (12).

At the known temperature, the system (1) can be transformed to the one analogous to the system describing the YAG:Nd/YAG:Cr laser generation [12]. Designating

the inversion in the generating medium as $N_g = N_{g_u} - fN_{g_l}$, and the effective cross-section of the laser transition as $\sigma_{g_e} = f_{u_1}\sigma_g$ and $f = f_{l_3}/f_{u_1}$, one can reduce (1) to:

$$\frac{\mathrm{d}N_g}{\mathrm{d}t} = (1+f)R - \frac{fN_{g_{\text{total}}} + N_g}{\tau_g} - \frac{(1-f)\sigma_{g_e}c_0}{V'}qN_g \tag{13a}$$

$$\frac{\mathrm{d}N_a}{\mathrm{d}t} = \frac{N_{a_{\text{total}}} - N_a}{\tau_{a_2}} - \frac{\sigma_{a_1}c_0}{V'}qN_a \tag{13b}$$

$$\frac{\mathrm{d}q}{\mathrm{d}t} = \left[2\sigma_{g_e}l_gN_g - 2\sigma_{a_1}l_aN_a - 2\sigma_{a_2}l_a(N_{a_{\text{total}}} - N_a) - 2\gamma\right]\frac{q}{t_r} + \\ + \varepsilon(f_{u_1}N_{g_u} - f_{l_3}N_{g_l} + N_{g_{\text{total}}})c_0\sigma_g\frac{l_g}{l'} \tag{13c}$$

The rough solutions of (13) can be obtained in the similar manner as [12] for YAG:Nd/YAG:Cr laser [12], *i.e.*, by neglecting of pumping and spontaneous transitions during the generation. In this case one can obtain the following expressions for the peak power $P_{\max}$ and the energy in the laser pulse E:

$$P_{\max} = \frac{h\nu A_e l_g}{(1+f)t_r}\ln\left(\frac{1}{R_1R_2}\right)\left\{N_{g_m} - N_{g_t} - (1+f)\frac{N_{a_{\text{total}}}l_a}{l_g}\left(1 - \frac{\sigma_{a_2}}{\sigma_{a_1}}\right)\times\right. \\ \left.\times\left[1 - \left(\frac{N_{g_t}}{N_{g_m}}\right)^{\sigma_{a_1}/\sigma_g}\right]\frac{\alpha l - \ln(R_1R_2) + \sigma_{a_2}l_aN_{a_{\text{total}}}}{\sigma_{g_e}l_g}\ln\left(\frac{N_{g_m}}{N_{g_t}}\right)\right\} \tag{14}$$

$$E = \frac{h\nu A_e}{2(1+f)\sigma_{g_e}}\ln\left(\frac{1}{R_1R_2}\right)\ln\left(\frac{N_{g_m}}{N_{g_f}}\right) \tag{15}$$

where N_{g_m} is the maximal inversion achieved in the generating medium before the generation of the pulse; this value is in the region from the initial inversion corresponding to the equality between the amplification and the losses in the resonator

$$N_{g_i} = \frac{1}{\sigma_{g_e}l_g}\left[\sigma_{a_1}l_aN_{a_{\text{total}}} + \alpha l - \frac{1}{2}\ln(R_1R_2)\right] \tag{16}$$

to the inversion $N_{g_{\max}} = R\tau_g$ which is maximal achievable at the given pumping rate R, N_{g_t} is the inversion corresponding to the maximum of the power in the pulse that can be determined from the equation

$$\sigma_{g_e} l_g N_{g_t} - \alpha l + \frac{1}{2}\ln(R_1 R_2) - \sigma_{a_2} l_a N_{a_{\text{total}}} +$$

$$- (\sigma_{a_1} - \sigma_{a_2}) l_a N_{a_{\text{total}}} \left(\frac{N_{g_t}}{N_{g_m}}\right)^{\sigma_{a_1}/\sigma_{g_e}} = 0 \tag{17}$$

where N_{g_f} is the residual inversion that can be calculated from:

$$N_{g_m} - N_{g_f} - (1+f) N_{a_{\text{total}}} \frac{l_a}{l_g} \left(1 - \frac{\sigma_{a_2}}{\sigma_{a_1}}\right) \left[1 - \left(\frac{N_{g_f}}{N_{g_m}}\right)^{\frac{\sigma_{a_1}}{(1+f)\sigma_{g_e}}}\right] +$$

$$- \frac{\alpha l - \frac{1}{2}\ln(R_1 R_2) + \sigma_{a_2} l_a N_{a_{\text{total}}}}{\sigma_{g_e} l_g} \ln\left(\frac{N_{g_m}}{N_{g_f}}\right) = 0 \tag{18}$$

Contrary to the case of the fourth-level laser [12], the inversions N_{g_i}, N_{g_t}, N_{g_f} are essentially dependent on temperature via the factor f and the effective cross-section σ_{g_e}.

The repetition rate F is inversely proportional to the time needed for inversion increasing from N_{g_f} to N_{g_m} and, as it follows from (1) at $q = 0$, is equal to:

$$F = \left\{ \tau_g \ln\left[\frac{(1+f)R\tau_g - N_{g_f} - f N_{g_{\text{total}}}}{(1+f)R\tau_g - N_{g_m} - f N_{g_{\text{total}}}}\right] \right\}^{-1} \tag{19}$$

For the approbation of the model, both analytical and numerical calculations are carried out for YAG:Yb/YAG:Cr laser described in [14]. As it is shown, at the initial transmittance of the absorber $T_0 = 0.96$, the losses $\gamma_i = 0.188$, the absorbed pumping power 2.5 W, the pumping beam radius 84.5 μm, the calculated laser radiation parameters are: $P_{\max} = 10$ kW, $E = 10.8$ μJ, $t_i = 1.08$ ns, $F = 63.2$ kHz that is close to the experimental values $P_{\max} = 8$ kW, $E = 10.8$ μJ, $t_i = E/P_{\max} = 1.35$ ns, $F = 63$ kHz.

3. The optimization of YAG:Yb/YAG:Cr microchip laser

The problem of optimization of the YAG:Yb/YAG:Cr microchip laser is studied previously [10] under the assumption of the fourth-level generation scheme of YAG:Yb. The aim function was the energy in the laser pulse E and the parameters of optimization were the output mirror reflectivity R_2, the phototropic centers concentration $N_{a_{\text{total}}}$, the absorber thickness l_a and the pumping beam radius w_p. Here we modify this opti-

mization algorithm taking into account the quasi-three-level character of generating medium.

3.1. Optimization on the initial transmission of the absorber and the output mirror reflectivity

As it follows from Eq. (15), the energy in the laser pulse is higher, the higher is the initial inversion in the generating medium N_{g_m}. From the other hand, the maximal inversion achieved at the given pumping rate R is $N_{g_{\max}} = R\tau_g$. Obviously, the inversion is higher, the higher is the nonlinear losses in the absorber, *i.e.*, the lower its initial transmission $T_0 = \sigma_{a_1} l_a N_{a_{\text{total}}}$. In fact, the generation of the laser pulse starts when the amplification in the generating medium is equal to the losses, $\alpha_{\text{gain}} \equiv \sigma_{g_e} l_g N_g = \alpha_{\text{losses}}$. If they are low, this condition can be fulfilled at the inversion significantly lower than $N_{g_{\max}}$. Thus the decrease in the absorber initial transmission leads to an increase in the energy in the pulse. However, an essential decrease in T_0 may lead to the situation when the generation condition $\alpha_{\text{gain}} = \alpha_{\text{losses}}$ or

$$2\sigma_{g_e} l_g N_g = 2\sigma_{a_1} l_a N_{a_{\text{total}}} + 2\alpha(l_g + l_a) - \ln(R_1 R_2) \tag{20}$$

is not satisfied at the fixed pumping rate R and the output mirror reflectivity R_2. Obviously, the maximal value of the energy in the laser pulse will be achieved if the losses in the absorber allow to achieve the maximal value of the inversion $N_g = N_{g_{\max}}$. It is illustrated by Figs. 2**a** and 2**b**, where the dependences of the energy on the initial transmission T_0 and the output mirror reflectivity R_2 are presented for two different temperatures of the laser crystal. As it is seen from the figures, the region of T_0 and R_2 values is divided into two subregions, one of them corresponds to the pres-

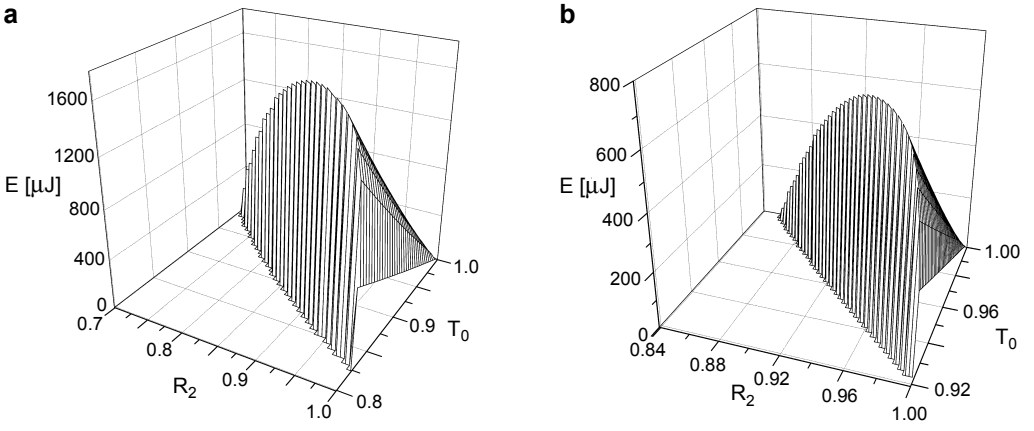

Fig. 2. The laser pulse energy dependences on the output mirror reflectivity R_2 and the initial transmission T_0 at the temperatures of 298 K (**a**) and 350 K (**b**) at the pumping power $P_i = 5$ W, the pumping beam radius $w_p = 0.2$ mm, the generating medium length $l_g = 1$ mm, the activator concentration $N_{g_{\text{total}}} =$ = 10 at.%, the phototropic centers concentration $N_{a_{\text{total}}} = 1\times10^{19}$ cm^{-3}.

ence of the generation and the other – to its absence. The maximal values of the energy are realized near the boundary between them, defined, as it follows from Eq. (20), by:

$$T_0 = \left[\frac{1}{\sqrt{R_1 R_2}} \exp(-\sigma_{g_e} l_g N_{g_{\max}} + \alpha l_g) \right]^{\frac{1}{1 + \alpha/\sigma_{a_1} N_{a_{\text{total}}}}} \tag{21}$$

This equation establishes a connection between the optimal values of the initial transmission and the output mirror reflectivity.

The essential peculiarity of the quasi-three-level laser is a decrease in the maximal achievable inversion $N_{g_{\max}}$ and the effective cross-section σ_{g_e} with temperature increasing. In turn, it leads to a decrease in the highest achievable energy in the pulse that is caused by contraction of the region where the generation is possible, what is evident from the comparison of Figs. 2**a** and 2**b**.

The dependences of the energy in the laser pulse on the output mirror reflectivity at the initial transmission connected with R_2 by Eq. (21) in each point are shown in

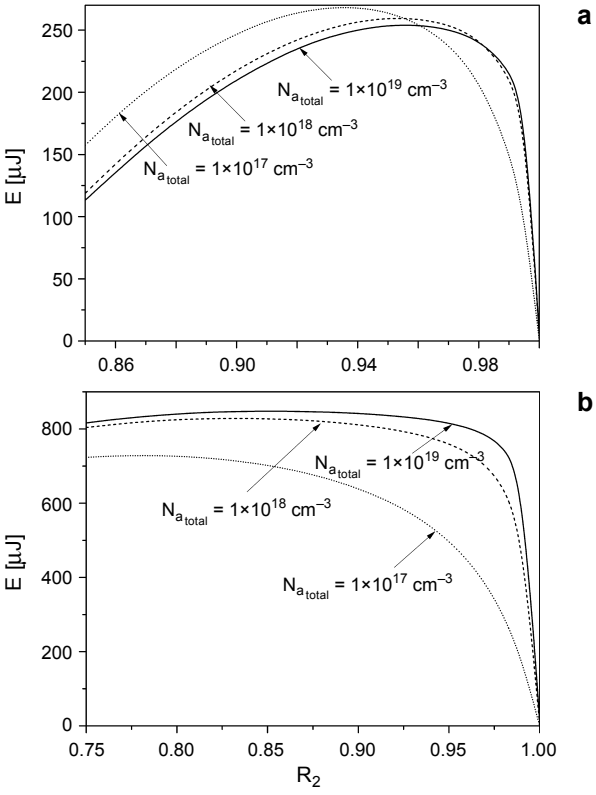

Fig. 3. The dependences of the energy in the laser pulse on the output mirror reflectivity R_2 at the optimal value of the absorber initial transmission T_0 for different values of the concentration of the phototropic centers at 298 K (**a**) and 100 K (**b**) and P_i = 1.12 W, w_p = 0.1 mm, $N_{g_{\text{total}}}$ = 10 at.%.

Fig. 3. Because the same value of T_0 may correspond to different values of the phototropic centers concentration, the calculations are carried out for three different values of $N_{a_{\text{total}}}$. As it is seen from Figs. 3**a** and 3**b**, the optimal values of R_2 are found in the range from 0.8 to 0.97, at that the higher the temperature, the higher the optimal output mirror reflectivity is. At RT the energy in the pulse decreases by about 5% with an increase in $N_{a_{\text{total}}}$ from 10^{17} to 10^{19} cm^{-3} (Fig. 3**a**) accompanied by the simultaneous increase in the absorber thickness. This peculiarity is connected with the presence of the thermal occupation of the lower laser level: particularly, if the laser is cooled down to 100 K, the dependence $E_{\max}(N_{a_{\text{total}}})$ becomes opposite and qualitatively the similar to the one of the fourth-level laser (Fig. 3**b**).

3.2. The optimization of the pumping beam radius

The maximal inversion achieved in the passively Q-switched quasi-three-level laser is

$$N_{g_{\max}} = (1+f)R\tau_g - fN_{g_{\text{total}}} = (1+f)\frac{\eta P_i}{l_g \pi w_p^2 h\nu_p}\tau_g - fN_{g_{\text{total}}} \tag{22}$$

Obviously, this value cannot exceed the concentration of the active centers in the generating medium, $N_{g_{\max}} \le N_{g_{\text{total}}}$. Setting here the equality, one can obtain the condition for determination of the pumping power density $P_i\, l_g^{-1}\pi^{-1}w_p^{-2}$ that ensures the achievement of the highest possible inversion. This condition can be transformed to the one for the optimal value of the pumping beam radius analogous to the one for the fourth-level laser [10]:

$$w_p = \sqrt{\frac{P_i\left[1-\exp(-2\alpha_g l_g)\right]\tau_g}{\pi l_g N_{g_{\text{total}}} h\nu_p}} \tag{23}$$

The dependences of the peak power and the energy in the pulse of YAG:Yb/YAG:Cr laser on the pumping beam radius at different values of l_g are shown in Figures 4**a** and 4**b**. As it is seen, the values of the peak power and the energy achieved in maxima increase with an increase in the generating medium thickness. However, an increase in the energy due to the increase in l_g is limited by the violation of the single-frequency generation condition at the sufficiently high values of l_g. So here we do not optimize the laser on this parameter but fix it on the value of 1 mm.

3.3. The algorithm of the microchip YAG:Yb/YAG:Cr laser optimization

Thus the optimization of the microchip YAG:Yb/YAG:Cr laser can be carried out in the following sequence. For each value of the pumping power P_i the optimal pumping beam radius is calculated from Eq. (23). Then the optimal output mirror reflectivity R_2 and the initial transmission T_0 concerned with R_2 by Eq. (21) are determined from

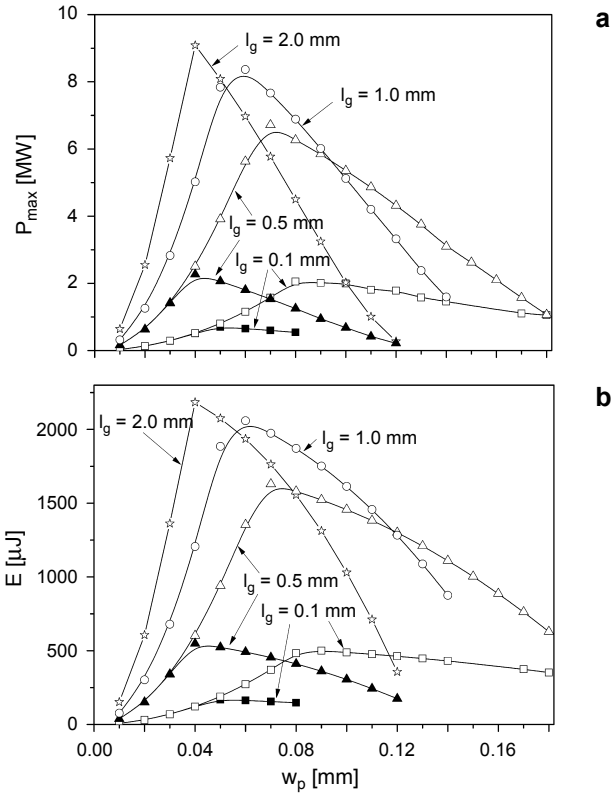

Fig. 4. The dependences of the peak power (**a**) and the energy in the pulse (**b**) of the YAG:Yb/YAG:Cr, Mg laser on the pumping beam radius w_p at different values of the generating medium thickness l_g and the pumping power P_i. The black symbols correspond to the dependences obtained for the pumping power of 1 W, the light ones – for 3 W.

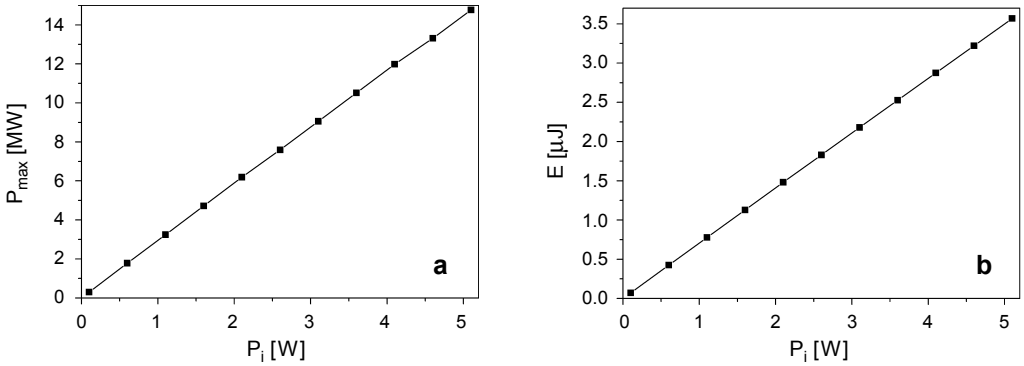

Fig. 5. The dependences of the peak power (**a**) and the energy (**b**) of YAG:Yb/YAG:Cr laser on the pumping power obtained after optimization.

$E(R_2)$ dependence. At that the concentration of the phototropic centers can vary in the sufficiently wide limits in accordance with the technological convenience.

The dependences of the peak power and the energy in the pulse of YAG:Yb/YAG:Cr laser on the pumping power obtained after optimization for each value of P_i are shown in Figs. 5**a** and 5**b**. As it is seen from the figures, the optimized energy in the pulse and the corresponding peak power grow linearly with pumping power increasing. The values of the peak power obtained after optimization are in the limits from the tenth of units up to 15 MW and the values of the energy in the pulse are equal to the one tenth to the units of mJ.

4. The influence of heating on spatial parameters of the laser mode

The main factors determining the spatial characteristics of the microchip laser radiation are the non-uniformities of the refractive index and the strains caused by heating. Therefore the influence of heating on the spatial characteristics of the radiation was estimated by the consecutive determination of the temperature distribution, the distributions of the refractive index and thermo-mechanical deformations, the parameters of the ABCD-matrix, the beam waist radius w and the divergence 2θ. The calculated dependences of these values are shown in Figs. 6**a** and 6**b**.

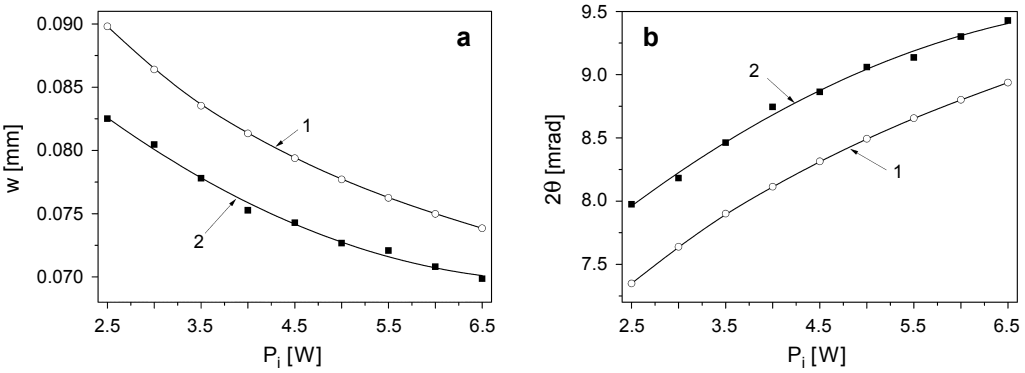

Fig. 6. The dependences of the laser beam waist w and the divergence 2θ on the pumping power P_i for YAG:Yb/YAG:Cr microchip laser; curves 1: the deformations of the crystal edges are neglected, curves 2: the deformations are taken into account. The pumping beam radius for all points is 0.15 mm.

As it is seen from the figures, the radius of the laser beam waist decreases from 83 to 70 μm and the divergence increases from 8.0 to 9.4 mrad if P_i increases from 2.5 to 6.5 W, which is obviously caused by an increase in the non-uniformity of the temperature distribution. The main contribution to the changes of the laser beam parameters is produced by the temperature changes of the refractive index: the contribution of deformations is about 7% for both dependences. The obtained values of the divergence correspond to the ones observed for microchip lasers (units of mrad).

5. Conclusions

The approach to modeling of the microchip passively *Q*-switched quasi-three-level YAG:Yb/YAG:Cr laser is proposed. The influence of heating on the characteristics of the laser radiation is determined by using the iteration scheme of the simultaneous solving of the rate and the heat conductivity equations. This approach is used for optimization of the microchip YAG:Yb/YAG:Cr laser on the value of the energy in the laser pulse. As it is shown, the maximal energy in the pulse is achieved if the laser generation takes place just above the threshold, which essentially depends on the temperature of the laser crystal. The generation condition allows to reveal the connection between the optimal values of the absorber initial transmission and the output mirror reflectivity. If the other parameters are fixed, the maximal energy is achieved at the optimal value of the pumping beam radius determined by the pumping power, the generating medium length and the maximal reachable inversion. The linearity of the dependences of the peak power and the energy in the pulse on the incident pumping power P_i gives the possibility of the simple estimation of their highest achievable values at the arbitrary values of P_i. The values of the radius of the laser beam waist are equal to 70–80 μm and the values of its divergence – to 8.0–9.4 mrad, at that the waist radius decreases and the divergence increases with pumping power increasing.

References

[1] KASAMATSU T., SEKITA H., KUWANO Y., *Temperature dependence and optimization of 970-nm diode-pumped Yb:YAG and Yb:LuAG lasers*, Applied Optics **38**(24), 1999, pp. 5149–5153.

[2] JUN DONG, PEIZHEN DENG, JUN XU, *Spectral and luminescence properties of Cr^{4+} and Yb^{3+} ions in yttrium aluminium garnet (YAG)*, Optical Materials **14**(2), 2000, pp. 109–113.

[3] PATEL F.D., HONEA E.C., SPETH J., PAYNE S.A., HUTCHESON R., EQUALL R., *Laser demonstration of $Yb_3Al_5O_{12}$ (YbAG) and materials properties of highly doped Yb:YAG*, IEEE Journal of Quantum Electronics **37**(1), 2001, pp. 135–144.

[4] HÖNNINGER C., PASCHOTTA R., GRAF M., MORIER-GENOUD F., ZHANG G., MOSER M., BISWAL S., NEES J., BRAUN A., MOUROU G.A., JOHANNSEN I., GIESEN A., SEEBER W., KELLER U., *Ultrafast ytterbium-doped bulk lasers and laser amplifiers*, Applied Physics B **69**(1), 1999, pp. 3–17.

[5] KALISKY Y., LABBE C., WAICHMAN K., KRAVCHIK L., RACHUM U., DENG P., XU J., DONG J., CHEN W., *Passively Q-switched diode-pumped Yb:YAG laser using Cr^{4+}-doped garnets*, Optical Materials **19**(4), 2002, pp. 403–413.

[6] JUN DONG, PEIZHEN DENG, YUPU LIU, YINGHUA ZHANG, JUN XU, WEI CHEN, XINGLONG XIE, *Passively Q-switched Yb:YAG laser with Cr^{4+}:YAG as the saturable absorber*, Applied Optics **40**(24), 2001, pp. 4303–4307.

[7] SUMIDA D.S., FAN T.Y., *Room-temperature 50-mJ/pulse side-diode-pumped Yb:YAG laser*, Optics Letters **20**(23), 1995, pp. 2384–2386.

[8] SPÜHLER G.J., PASCHOTTA R., KULLBERG M.P., GRAF M., MOSER M., MIX E., HUBER G., HARDER C., KELLER U., *A passivle Q-switched Yb:YAG microchip laser*, Applied Physics B **72**(3), 2001, pp. 285–287.

[9] LU M., CHATWIN C.R., YOUNG R.C.D., BIRCH P.M., *Numerical simulation of a CW-pumped Cr:YAG passively Q-switched Yb:YAG pulsed laser*, Optics and Lasers in Engineering **47**(6), 2009, pp. 617–621.

[10] BURYY O.A., UBISZKII S.B., MELNYK S.S., MATKOVSKII A.O., *The Q-switched Nd:YAG and Yb:YAG microchip lasers optimization and comparative analysis*, Applied Physics B **78**(3–4), 2004, pp. 291–297.

[11] GUOHUA XIAO, BASS M., *A generalized model for passively Q-switched lasers including excited state absorption in the saturable absorber*, IEEE Journal of Quantum Electronics **33**(1), 1997, pp. 41–44.

[12] MIERCZYK Z., *Nieliniowe absorbery: badania właściwości, technologia i wybrane zastosowania*, Wojskowa Akademia Techniczna, Warszawa, 2000, pp. 145–154, (in Polish).

[13] BURYY O.A., SUGAK D.Y., UBIZSKII S.B., IZHNIN I.I., VAKIV M.M., SOLSKII I.M., *The comparative analysis and optimization of the free-running Tm^{3+}:YAP and Tm^{3+}:YAG microlasers*, Applied Physics B **88**(3), 2007, pp. 433–442.

[14] DONG J., SHIRAKAWA A., UEDA K.-I., *Sub-nanosecond passively Q-switched Yb:YAG/Cr^{4+}:YAG sandwiched microchip laser*, Applied Physics B **85**(4), 2006, pp. 513–518.

Received March 21, 2014
in revised form July 17, 2014